# Novel Fractal-Wavelet Technique for Denoising Side-Scan Sonar Images

FU-TAI WANG[1], C.-Y. JENNY LEE[2], HSIAO-WEN TIN[2] , SHAO-WEI LEU[3], CHAN-CHUAN WEN[4], and SHUN-HSYUNG CHANG[2*]

[1] Department of Electrical Engineering,
Hwa Hsia Institute of Technology
[2] Department of Microelectronics Engineering,
National Kaohsiung Marine University
[3] Department of Electrical Engineering,
National Taiwan Ocean University
[4] Department of Shipping Technology,
National Kaohsiung Marine University
Taiwan, R.O.C.
stephenshchang@mac.com http://60.249.147.181/oceaner/Main/index56.aspx

*Abstract:* - Side-scan signals collected from the seabed are constructed based on elements of bottom roughness, which vary in texture and in the time they are collected. Image denoising, A procedure used for extracting image texture information and removing or reducing as much noise as possible, is a difficult problem. This study proposes a denoising algorithm based on an elaborative approach for measuring image roughness as an alternative to the fractal-wavelet (FW) coding process. By using this approach, texture similarity can be effectively captured. Because roughness is a property used to qualify image texture and a fractal dimension (FD) can be used to indicate the degree of complexity of image roughness, this study proposed an approach, namely the roughness entropy FD (REFD) method, for measuring the distribution of roughness in an image. This study applied the REFD algorithm to the FW coding process as the REFD FW algorithm. The proposed denoising algorithm approximates the parts of a noise-free image by determining the similarity distance between the two REFD values of domain-range subtrees, discarding as much noise as possible. The minimal similarity distance is used to quantify the degree of texture similarity between domain-range subtrees. This study conducted experiments on three side-scan sonar images of an undersea pipeline that were captured in Taiwan using a Polaris camera in various configurations in order to investigate the corresponding quality of the images by using two error criteria: mean square error and the peak signal-to-noise ratio. The experimental results indicated that the REFD is useful for range-domain matching in an FW coder to approximate the experimental images effectively. The proposed REFD FW algorithm is adaptable in denoising side-scan sonar images, and the images are more visually appealing.

*Key-Words:* - Fractal dimension, fractal-wavelet denoising, image denoising, image roughness, self-similarity, side-scan sonar images

## 1 Introduction

Side-scan sonar has become an essential tool for canvassing the ocean bottom in ocean geographic studies in order to inspect objects on the sea bottom and investigate hazards [1]. In addition, side-scan sonar is widely used for investigating fishery resources in current fishing industries [2]. The considerable acoustic noise in underwater environments affects sonar signals and interferes with the collection process. The presence of acoustic noise distorts and degrades the accuracy of information extracted from sonar images. Eliminating or reducing noisefrom sonar images before using those images is critical. Sonar image denoising and noise reduction have been commonly discussed in the literature (e.g., [3]–[5]).

Image denoising techniques are designed to suppress noise efficiently while retaining essential image features; such techniques could thus considerably benefit numerous sonar applications. Whether an image can be denoised using fractal image coding depends on whether that fractal image

coding is lossy. Fractal image coding involves identifying a satisfactory collage, which is the approximation obtained when all fractal transformations are applied to the original image. Noise is not self-similar and is eliminated during fractal transformation. This explains why fractal image denoising is accompanied by a lossy compression process. Compared with optical images, sonar images are low-frequency images that are characterized by little detail. The background noises of sonar images are high-frequency impulse noises that yield higher amplitudes compared with those of echoes from the target area. Since the previous decade, the wavelet coding technique has been successfully applied to sonar image denoising and recognition [6], [7]. The wavelet coding technique consists of both transform and subband coding. The wavelet transform decomposes images into multiple levels at multiple resolutions and frequencies. The characteristics of inherently noisy sonar images suggest that wavelet-based compression is a viable choice for denoising sonar images. Recently, a study investigated the ability of fractal image coding to denoise images other than compression images [8]. To use fractal image coding to denoise an image, noise cannot be self-similar or must be eliminated during fractal transformation. Fractal-wavelet (FW) schemes are inspired by applying the fractal image coding technique in the wavelet domain during the wavelet transformation of noisy images [9], [10]. The FW technique has been successfully applied to reduce noise in side-scan sonar images [3], [11].

Side-scan signals collected from the seabed primarily reflect several elements of the seabed and represent its roughness, which is related to texture. Texture is regarded as a similarity grouping in an image. Efficiently extracting texture is an effective approach to classifying and identifying no table information on areas. Fractal dimensions (FDs) are widely used in texture analysis [12]. Roughness is one of the perceived properties of image texture and is both irregular in shape and randomly distributed. FDs are suitable for estimating roughness and have been successfully applied to measure texture quantitatively [13].In addition, roughness is one of the perceived properties used to qualify image texture. A newly designed FD for extracting and analyzing image roughness is introduced by considering the roughness entropy FD (REFD) algorithm. The REFD value represents the distribution of image roughness so that the feasible FD representing the texture features can be extracted from the images. This study was motivated by an observation: an FD is an expression of an image in surface stability and the texture information of an image can be described by the distribution of image roughness; once this is performed, FD texture features can be extracted.

This study proposes a texture-based FW coding algorithm based on the REFD, namely the REFD FW algorithm, for denoising sonar images. The REFD FW algorithm incorporates the REFD to identify each range subtree for the optimal matched domain subtree according to the optimal minimal distance of texture similarity measurements. The minimal similarity distance quantifies the degree of texture similarity between domain-range subtrees. The REFD FW algorithm may enable a multiresolution frequency analysis of image texture to be performed. Thus, REFDs of images of various frequencies can be received at different scales, and texture information can be acquired in the horizontal, vertical, and angular directions; few other texture analysis methods allow this. Using texture similarity, the proposed REFD algorithm identifies the appropriate domain subtrees, approximates domain-range subtrees, and denoises while preserving image texture information.

The remainder of this paper is organized as follows: Section II presents an overview of fractal techniques and presents the wavelet-fractal image denoising scheme, Section III introduces the proposed sonar image denoising algorithm based on the wavelet-fractal image denoising scheme, and Section IV presents the experimental results and concludes the paper. The experimental results are discussed in terms of the metric of mean square error (MSE) and the peak signal-to-noise ratio (PSNR), and a brief conclusion is presented in the final section.

## 2 Fractal and Wavelet-based Image Denoising Technology

In the early 1960s, Mandelbrot revealedhow fractal sets could be regarded as the limits of iteration involving generators based on the concept of self-similarity [14]. In the late 1980s, Bernesly [16] and Jacquin [15] pioneered fractal block coding. However, the matching process in fractal block coding, which involves determining a match from a group of domain blocks to a range block, is generally a time-consuming task that occupies most of the encoding time. Some improvements were achieved by reducing the domain pool size [17], [18]. The combination of fractal block coding and wavelets has been widely applied. In the early 1990s,

Pentland and Horowitz [19] were the first to mention such a link. David [20] published a notable paper on linking wavelet and fractal image coding in 1998. Davis was the first to introduce the wavelet subtree, which consists of wavelet coefficients of the same spatial location and orientation but with different resolutions.

### 2.1 Fractal Block Coding and Fractal Denoising

Fractal block coding is used to approximate an image based on the subblocks of that image. The basic theory of Jacquin's fractal block coding is discussed as follows.

Let I be a gray-level image. In fractal block coding, image I is partitioned into N range blocks $R_i \subseteq I$, for i = 1, 2…, N, and M domain blocks $D_j \subseteq I$, for j = 1,2,…, M, where the size of each domain block is twice that of each range block. To encode an image according to its self-similarity, each range block locates the domain block most similar to itself from the domain pool based on minimal MSE criteria. The search for the optimal matched domain block $D_j$ is performed using a local affine transformation $w_i$, such that $w_i : D_j \to R_i$, for i = 1,2, …, N and j = 1, 2, …, M. Theoretically, the union of the local affine transformations for all of the range blocks forms the affine transformation $\tau$ for the whole image, as expressed in (1).

$$\tau = \bigcup_{i=1}^{N} w_i \quad (1)$$

In practice, each local affine transformation $w_i$ is performed such that $R_i \approx w_i\left(D_j\right)$. Image encoding is achieved by first generating a fractal code for each range block $R_i$ based on the optimal matched domain block $D_j$ and then storing the fractal code into the codebook. Fractal codes recorded in the codebook can later be used in the iterative process of range approximation to restore the image.

Natural image structures exhibit similarities at various resolution scales. This feature renders the images suitable for encoding using fractal image coding methods. However, irregular textures and noise structures are unlike other parts of the image and therefore are not encoded using fractal block coding. The fractal code for denoising an image must be constructed such that the original image is approximated as much as possible and all of the noisy parts are discarded.

### 2.2 Basics of Fractal-Wavelet Denoising

Quad tree fractal coding, suggested by Fisher [21], is a hierarchical segmentation-based coding scheme that has been widely used and investigated [9], [20]. Primarily, the scheme identifies optimal matched domain subtrees and approximates domain-range subtrees by using the proper affine transform, common scaling factors, and three fundamental coefficient trees—the horizontal, vertical, and diagonal. However, this method results in a loss of image fidelity. Davis [20] provided a frequently used tool kit that is considerably useful in conducting experiments.

Ghazelet al. [9] considered the coefficients of three subtrees independently in proposing a FW denoising scheme. The scheme involves selecting the optimal parent subtree such that the collage error, which is based on the MSE of the noiseless image, is minimized. This ensures the accuracy of the criterion for collage-based matching for the original noise-free image.

Typically, FW decoding begins with a wavelet coefficient tree that contains stored wavelet coefficients and zeros. Iterations of the FW scaling and copying procedure are performed, producing a fixed point wavelet coefficient matrix that approximates the original image. A small collage distance indicates a favorable approximation [10]. The collage coding procedure used to produce the FW code for an image proceeds as follows: First, consider a fixed set of parent-child level values. Then, for each encoded child subtree, locate the parent subtree and the corresponding scaling coefficient so that the collage distance is minimized.

## 3 REFD FW Denoising

Roughness is a property used to qualify image texture. FDs are useful for measuring the degree of roughness of surface texture. Based on these concepts, this study proposes a novel FD approach for measuring image roughness, namely the REFD algorithm. The REFD was designed to extract roughness properties efficiently by acquiring the FD of an image, which is reflective of the roughness of an image texture. The REFD is described in the first subsection.

The REFD FW estimates the domain-range matching based on the relative degree of texture similarity. In practice, the smallest distance between the two REFD values of subtrees is located in high-

and low-frequency subbands. The encoding is performed in an affine transformation defined using Jacquin's notation [15]. The affine transformations between domain and range subtrees somewhat reduce the variance in the noise because the noisy contents are dissimilar. Denoising is accompanied by fractal block coding to eliminate noise that is not self-similar or eliminated during the affine transformation. The denoising algorithm is described in Subsection 3.2.

## 3.1 Roughness Entropy Fractal Dimension Method

The REFD method was designed to extract roughness properties by acquiring the FD of an image. The development of the REFD was motivated by the allometric relationship between the roughness node number and path length of compounds. The REFD clusters subsequently structure the image roughness based on a two-connectivity rule, in which the structured cluster is called a compound. This study determined the FD of a compound according to a structure that was quantified using the Horton-Strahler order scheme [22]. Shannon's entropy was introduced for integrating the FDs of the compound into an FD of an image in which the entropy indicated the contribution of roughness information on the compound; in other words, to reveal the importance of the same type of compound for the image roughness. The derived FD summarized the complexity of image roughness as a single numerical value. The REFD is obtained using three steps.

### 3.1.1 Extraction of Image Roughness

In this study, image roughness was defined as a descriptor of pixel value variation between the pixels in a small neighborhood. In selecting the extraction method, a small neighborhood around each pixel is used to ensure that selection is simple and easy to code.

The surrounding pixels were defined as those pixels located adjacent to the current pixel in the vertical and horizontal directions. For current pixels located at edges or in corners, the nearest-neighbors search path, as shown in Fig. 1, was used to define the surrounding pixels. The extraction method involved setting the maximum and minimum among the surrounding pixels as the thresholds. When the value of the current pixel is greater than the maximum or less than the minimum, the current pixel is considered to indicate image roughness. For an image the size of $M \times N$, the extraction of image roughness is described as follows:

Let array Pat a size of $M \times N$ record the gray values of all of the pixels. Let array $P_r$ at a size of $M \times N$ record the image roughness, in which roughness is 1 and nonroughness is 0. Assume $P(x, y)$ is the current pixel, where $0 \le x < M-1,\ 0 \le y < N-1$. Let the surrounding pixels be $P_{right}$, $P_{left}$, $P_{down}$,and $P_{up}$. Consequently, the pixel exhibiting a maximal gray value is $P_{\max}$, and the pixel exhibiting a minimal gray value is $P_{\min}$. The formula for obtaining $P_{\max}$ and $P_{\min}$ is expressed as (2):

$$P_{\max} = Max\left(P_{right}, P_{left}, P_{down}, P_{up}\right)$$
$$P_{\min} = Min\left(P_{right}, P_{left}, P_{down}, P_{up}\right) \quad (2)$$

where function $Max(\ )$ and $Min(\ )$ disregard any null entry. To obtain the value of $P_r(x, y)$,(3) involves using $P_{\max}$ and $P_{\min}$ as the thresholds.

$$\begin{aligned} &if\ \left(P(x, y) > P_{\max} \quad or \quad P(x, y) < P_{\min}\right) \\ &\quad P_r(x, y) = 1 \\ &else \\ &\quad P_r(x, y) = 0 \end{aligned} \quad (3)$$

After analyzing all of the pixels, the image roughnesses are noted in $P_r$. The REFD is then used to group the roughnesses that are adjacent to each other into rectangular roughness clusters. The process of grouping is conducted to compare the roughnesses with neighbors. If one of its neighbors exhibit sroughness and does not belong to any cluster, it can be included in a cluster.

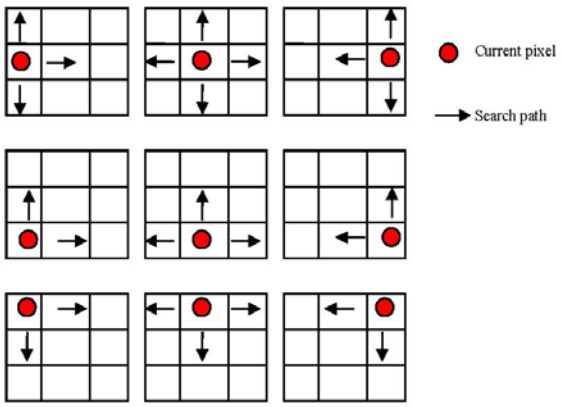


Fig. 1. Locating surrounded pixels

### 3.1.2 Calculation of Fractal Dimension for Each Compound

The REFD is used to construct a compound by structuring the image roughnesses in each cluster according to the two-connectivity rule. The construction procedures are described as follows: Let each image roughness have an order that defaults to one. Assume that a walker travels through the roughness clusters. When the walker walks over two adjacent image roughnesses, the walker constructs a node based on them. The node is called a roughness node, and its order is set one order higher than that of its foundation. The walker walks over again. When the walker encounters two adjacent nodes that have the same order, the walker constructs a new roughness node by using these two adjacent nodes. The order of the new node is set one level higher than that of its foundation. The walker repeatedly walks over until all of the roughness nodes are explored. In this study, the roughness compound was defined as a set of image roughnesses and roughness nodes, and all nodes were considered to contain elements in the same set. At the end of node transversal, the highest node order obtained is assigned the order of that compound. Consequently, compounds have a binary tree hierarchical structure.

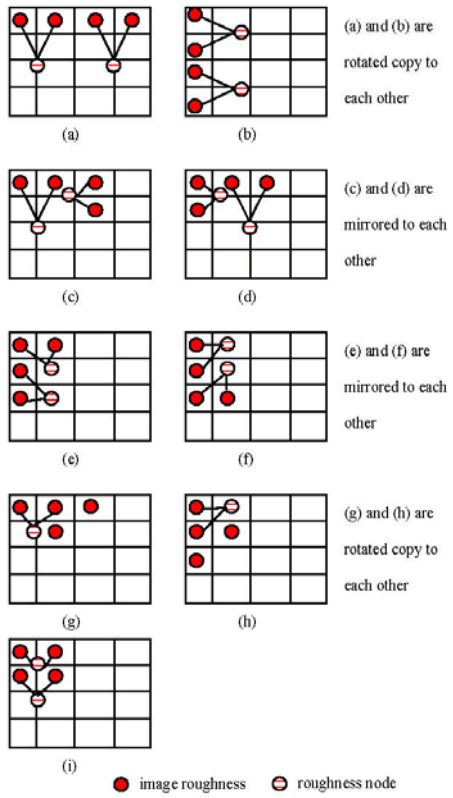


Fig. 2. Four image roughnesses may form nine various compounds.

The hierarchical structure of a compound depends on both the image roughness number and the permutation of image roughness. Fig. 2 illustrates various structures of compounds that are of the same number of image roughness, but of various distributions.

The REFD involves a method derived from Horton's laws [23] for computing the FD by considering two essential features, namely the number of roughness nodes and path length of roughness nodes. In this study, the average path length of roughness nodes was defined in the following manner: Let the path length of image roughness be 1. Let the path length of a roughness node of order $i$, where $i \geq 2$, be the product of the path length of roughness node of order $i-1$ and 2. Consequently, the average path length of roughness nodes of order $i$ is the total path length of those roughness nodes divided by the number of roughness nodes of order $i$.

An example is illustrated in Fig. 3. The compound illustrated in Fig. 3(a) contains five image roughnesses in order 1. Another compound illustrated in Fig. 3(b) contains four image roughnesses in Order 1. Each compound contains two roughness nodes at Order 2, and one roughness node in Order 3. Table 1 presents the average path lengths for image roughnesses and roughness nodes at various orders.

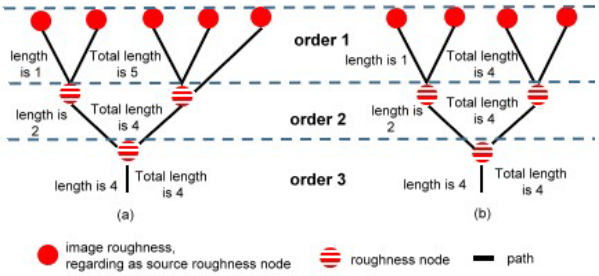


Fig. 3. Diagram of roughness node order.

Table 1. Roughness node numbers of Fig. 3 at each order

| order | Fig.3 (a) | | Fig.3 (b) | |
|---|---|---|---|---|
| | Number of roughness node | Average path length | Number of roughness node | Average path length |
| 1 | 5 | 1 | 4 | 1 |
| 2 | 2 | 2 | 2 | 2 |
| 3 | 1 | 4 | 1 | 4 |

The REFD is used to obtain the FD of a compound based on the ratio of roughness node

number and ratio of the average path length, and these two ratios are defined as follows:

Let $od\_r$ be the order and $N_{od\_r}$ be the number of roughness nodes of order $od\_r$. Accordingly, the ratio $R_n$ of the number of roughness nodes is defined as follows:

$$R_n = N_{od\_r+1} / N_{od\_r} \quad (4)$$

Let $L_{od\_r}$ be the average path length of order $od\_r$. The ratio $R_L$ of the average path length is defined as follows:

$$R_L = L_{od\_r+1} / L_{od\_r} \quad (5)$$

When the structure of a compound is a symmetric binary tree, by using (4) and (5), $R_n$ and $R_L$ are the same in each order. Fig. 3(b) shows an example.

For example, if a compound contains $N_1$ roughness nodes, then the number of roughness nodes in Order 2 is obtained as follows:

$N_2 = N_1 \times R_n$

If the structure of a compound is a symmetric binary tree, then the number of roughness nodes inOrder $k$ is indicated as follows:

$$N_k = N_1 \times R_n^{k-1} \quad (6)$$

Consequently, the average path length in Order $k$ is indicated as follows:

$$L_k = L_1 \times R_L^{k-1} \quad (7)$$

Apply logarithm to both sides of (7):

$$\log L_k = \log\left(L_1 \times R_L^{k-1}\right)$$

$$\log L_k = \log L_1 + (k-1)\log R_L$$

$$k-1 = (\log L_k - \log L_1)/\log R_L$$

$$k-1 = \log(L_k/L_1)/\log R_L$$

Substitute $k-1 = (\log L_k - \log L_1)/\log R_L$ to (6) and obtain

$$N_k = N_1 \times R_n^{(\log(L_k/L_1)/\log R_L)}$$

Based on the change-of-base formula of logarithm, $\log_b x = \log_a x / \log_a b$,

$$N_k = N_1 \times R_n^{(\log(L_k/L_1)/\log R_L)}$$

$$N_k = N_1 \times R_n^{\log_{R_L}(L_k/L_1)}$$

Based on the logarithm formula $a^{\log b} = b^{\log a}$,

$$N_k = N_1 \times R_n^{\log_{R_L}(L_k/L_1)}$$

$$N_k = N_1 \times (L_k/L_1)^{\log_{R_L} R_n}$$

Apply the change-of-base formula of logarithm again,

$$N_k = N_1 \times (L_k/L_1)^{(\log R_n/\log R_L)}$$

$$N_k = N_1 \times L_1^{-(\log R_n/\log R_L)} \times L_k^{\log R_n/\log R_L}$$

Because $L_1^{-(\log R_n/\log R_L)}$ and $N_1$ are constant, let $c = N_1 \times L_1^{-(\log R_n/\log R_L)}$,

$$N_k = c \times L_k^{(\log R_n/\log R_L)} \quad (8)$$

Equation (8), which represents the structure of a compound, is a power-law function and similar to the FD measure $N(l) \propto l^{-D}$, which represents Mandelbrot's fractal relationship, the details of which are described in[14]. Therefore, in this study, the FD of a compound was defined as follows:

$$D = \log(R_n)/\log(R_L) \quad (9)$$

Equation (9) indicates the relationship between the number of image roughnesses and average path length that can be described using a power-law function. In practice, the $R_L$ is a constant, and the linear regression approach is inapplicable for calculating the FD. Therefore, this study involved applying the geometric mean for calculating the average of $R_n$ and subsequently applying (9) to obtain the FD of a compound.

In general, most compounds are asymmetric binary trees. Fig. 3(a) illustrates an asymmetric binary tree. Although (9) is used to obtain the FD of a symmetric binary tree based on ideal numerical similarity by using mathematical calculation, Frontier suggested that the FD of a non homogeneous tree can be obtained using the same method applied to a symmetric binary tree [24]. Therefore, (9) is applicable to every compound regardless of its structure.

### 3.1.3 Calculation of the Image Fractal Dimension

The REFD is used to classify the compounds based on the order and number of image roughness. A set of classified compounds exhibiting low presence frequency can be the significant texture of that image for its specialness. This study involved assigning Shannon's entropy to the set of classified compounds based on information theory, in which the entropy is the information on the randomness of compounds. The REFD was used to obtain the FD of an image by summing the products of the FDs and entropies of the compounds in order to preserve the significances of the compounds in the image.

Assume that an image contains $n$ set of classified compounds $\{c_1, c_2, ..., c_n\}$. Consequently, the presence frequency of ith (i = 1, 2,..., n)set of compounds in that image is expressed as (10):

$$P_i = n\_c_i / total\_n\_C \quad (10)$$

where $n\_c_i$ is the number of ith set of compounds and $total\_n\_C$ is the total number of compounds in that image.

The information of the ith set of compounds exhibiting presence frequency $P_i$ is written as $I(c_i) = -\log(P_i)$. Shannon's entropy assigned to the

ith set of compounds is the product of $P_i$ and $I(c_i)$. Consequently, Shannon's entropy for the ith set of compounds is $P_i \times (-\log P_i)$. This study involved integrating these n FDs of the compound to form an FD of image $fE$. The $fE$ is obtained by using (11):

$$fE = -\sum_{i=1}^{n} P_i (\log P_i)\, fD_i \tag{11}$$

where $fD_i$ is the FD of the ith set of compounds obtained by using (9). The derived FD summarized the complexity of image roughness as a single numerical value.

### 3.2 The Roughness Entropy Fractal Dimension Fractal-Wavelet Denoising Method

Compare with fractal encoding described in Subsection 2.1, the affine transformation does not require an offset constant in wavelet domain fractal encoding because the wavelet tree does not have a constant offset. The size of a domain tree is reduced after down-sampling to match that of a range tree. The scale factor is multiplied with each wavelet coefficient of the domain tree to reach its correspondent range tree. A detailed description of the down-sampling of a domain tree and scaling factor is presented in [25]. The domain tree is then searched to locate the optimal matching domain subtree for a given range subtree.

In the method used in this study, the estimation of domain-range matching was based on the relative degree of texture similarity, as shown in Fig. 4. The range subtree is approximated by the affine grayscale transformations of domain subtrees, in which the byproduct of such approximation is a certain level of reduction in the noise. The approximation of a range block through a contracted domain block in the spatial domain is illustrated in Fig.5. The range subtrees were divided using a quad tree partitioning scheme into n levels of decomposition. Each level included one low-frequency subband and three high-frequency subbands in various directions. Fig.5 shows how a subtree is divided into four smaller subtrees by using a wavelet transform. Because the collage error was used as a dividing criterion, the maximal splitting depth could be used to reduce to a limited number depending on the image size and block size. The affine transformation mapping domain subtree into the corresponding range subtree was defined in [15]. The encoded parameters included the position of the domain tree and scaling factor. In this experiment, rotation and flipping were not implemented in affine transformation.

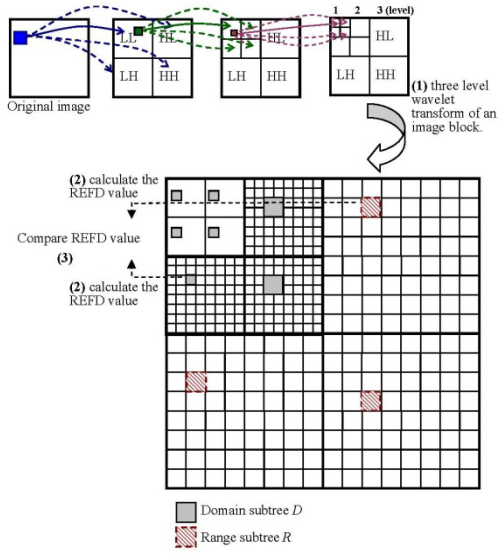


(1) Wavelet transform decomposes the image into two parts which respectively represent low frequency L and high frequency H, and then REFD and fractal block coding perform in the wavelet domain
(2) Obtain the sub-sampling domain block of resolution 2 in HL and calculate the REFD, and then compare to the REFD of the range block of resolution 1.
(3) If the differential of REFD value is the minimal, this domain block is selected as the best matched one for further affine transformation.

Fig. 4. Illustration showing REFD works in finding the appropriated domain subtrees to match the range subtrees.

The REFD FW algorithm is described as follows:

1) First the wavelet decomposes the image into a set of subbands in the LL, LH, HL, and HH directions at multiple resolutions. The depth of the wavelet decomposition is associated with the size of a subband. A subband of size $l \times l$ consists of three $(l/2)\times(l/2)$ smaller subbands at Resolution 1, three $(l/4)\times(l/4)$ smaller subbands at Resolution 2, …, and three $1\times1$ smaller subbands at Resolution $\log_2 l$. The depth $d$ can then be expressed as $d = 1+\log_2 l$. An example is illustrated in (1) and (2) of Fig. 6.
2) Split wavelet subbands in each resolution level into equal amounts of range blocks. The size of a range block is half the size of a block in the high subband at one level lower. Domain blocks at Resolution 1 are not used. Domain blocks are subsampled in the same size of a range block at a high frequency band

at one level lower. An example is illustrated in (3) and (4) of Fig. 6.

3) Obtain the REFD $fE^{\mathrm{R}}$ and $fE^{\mathrm{D}}$ by using (11) for each range subtree and domain subtree.
4) Then, calculate the $\Sigma\min\left(fE_i^R - fE_j^D\right)$ for each range subtree and domain subtree. The $jth$ domain subtree that yields the minimal value of $\Sigma\min\left(fE_i^R - fE_j^D\right)$ is referred to as the optimal match for the $ith$ range subtree.
5) To encode the image, the position of the optimal matched domain subtree for the current range block (i.e., transformed domain subtree) and scaling factor are stored in a code book. To restrict the experimental conditions, rotation and flipping were not implemented in this experiment as in [25].
6) To decode the compressed image, iterate the domain subtrees with the scaling factor to the destination. Then, inverse the wavelet transformation to obtain the approximation. The decompression process is based on an iterative SIMPLE algorithm and begins with a random initial image. This study involved using 10 iterations, as in [25], and obtained a decoded image.

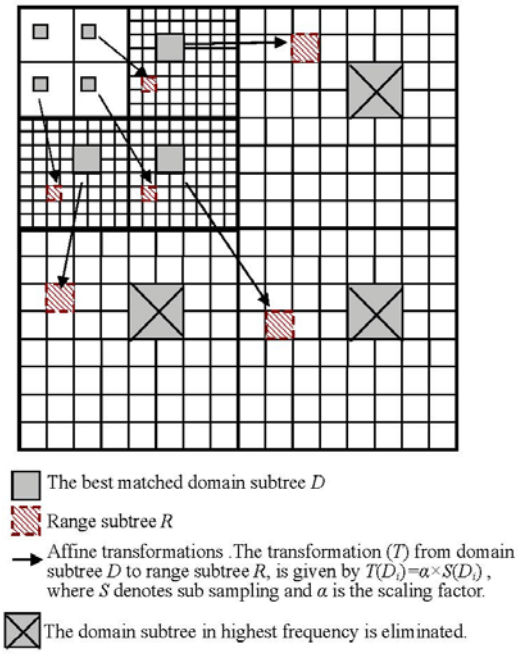


Fig. 5. The REFD FW algorithm finds each range subtree for its optimal matching domain subtree. The approximation of a range subtree through a contracted domain subtree can be done in the wavelet domain.

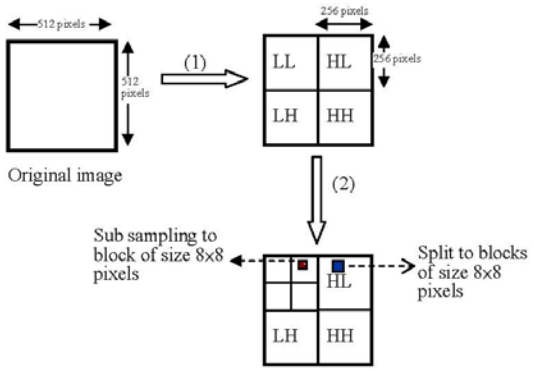


An example of splitting a 512x512 image into fractal blocks in the proposed fractal-wavelet method.

(1) Wavelet transform decomposes an image of size 512x512 pixels into first level which consists of 4 wavelet blocks of size 256x256 pixel.
(2) Wavelet transform decomposes low frequency band of size 256x256 pixels into second level which consists of 4 wavelet blocks of size 128x128 pixel.
(3) Split wavelet blocks in each level in equal amount 32x32of fractal blocks.
(4) Therefore, the wavelet block in the first level is split into small fractal blocks in 8x8 pixels. The wavelet block in the second level is split into small fractal blocks in 4x4 pixels.
(5) This paper sub-samples the domain blocks of the same size as the size of range block in the higher frequency band with one level less. the range block.

Fig. 6. From the high frequency subbands towards low frequency subbands, subband are split into range blocks of sizes 8x8 and 4x4, and the down-sampled domain blocks with the same block size of 8x8 and 4x4 are mapping the range blocks in the subbands with one level less.

# 4 Experimental Results and conclusion

## 4.1 Measuring Performance

The proposed denoising method was used to produce an approximation of the original noise-free image and its inaccuracy was measured for performance evaluation. Quantification is complex in practice because perceiving the inaccuracy of an approximation is difficult. The error accompanied by the approximation is termed the distortion. This study involved using two well-defined visual quality error criteria, the MSE and PSNR, to judge the ability of the procedure to denoise.

$$MSE = \frac{1}{N \times M} \sum_{x=0}^{N-1} \sum_{y=0}^{M-1} \left(B(x,y) - A(x,y)\right)^2 \quad (12)$$

where $A(x,y)$ is the gray value expression of the original image A and $B(x,y)$ is the gray value expression of the decoded image B. The images are of the same size $N \times M$ .

The PSNR is defined based on the MSE. In general, if the PSNR is sufficiently large, no perceptible difference between the reconstruction and original image would occur; a small PSNR would suggest that the images are unrelated. The PSNR commonly used for measuring the difference between two images was evaluated by relation

$$PSNR = 10 \log_{10} \frac{I_{\max}^2}{MSE} \tag{13}$$

where $I_{\max}$ is the highest intensity pixel in the image [25], which is 256 gray image.

## 4.2 Experimental Results

In the first experiment, the REFD algorithm was applied to two Brodatz's texture images for evaluating the FD obtained by the REFD algorithm to determine how effective the algorithmis in describing the complexity of image roughnesses.

Two texture images were set to 640 x640 pixels in this study, as illustrated in Fig. 7. Table 2 presentsthe experimental results of imagesD3 and D4. The results revealed the stated correlations. In both imagesD3 and D4, the rows of the compound orders were 2 and 3, indicating that the FD increased in conjunction with the number of image roughnesses. The rows of the image roughness were 4, indicating that the FD of the compound decreased as the order of the compound increased. In addition, the results indicated that the FD of a symmetric compound is an integer, such as the compounds presented in Table 2.

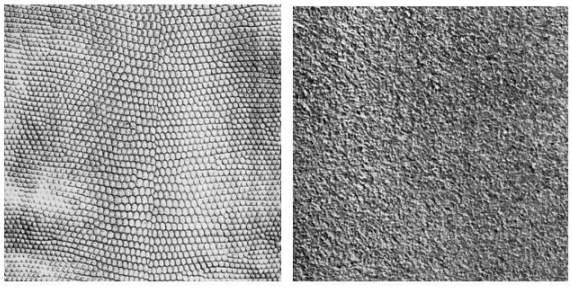


Fig.7. Brodatz texture images.

Table 2.

Computation results of fractal dimension of compounds of image D3 and D4

| D3 (FD value of REFD is 0.1389642) | | | D4 (FD value of REFD is 0.0926242) | | |
|---|---|---|---|---|---|
| FD of compound | order of compound | number of image roughness | FD of compound | order of compound | number of image roughness |
| 1 | 2 | 2 | 1 | 2 | 2 |
| 1.5849625 | 2 | 3 | 1.584963 | 2 | 3 |
| 2 | 2 | 4 | 2 | 2 | 4 |
| 1 | 3 | 4 | 1 | 3 | 4 |
| 1.160964 | 3 | 5 | 1.160964 | 3 | 5 |
| 1.2924813 | 3 | 6 | 1.292481 | 3 | 6 |
| 1.4036775 | 3 | 7 | - | - | - |
| 1.1531439 | 4 | 11 | - | - | - |

The experimental results indicated a number of correlations between the FDs of the compound, compound order, and roughness number described as follows:

1) For those compounds exhibiting the same roughness number, the compound in the small order carried a large FD.
2) For those compounds in the same order, the compound exhibiting a high roughness number carried a large FD.
3) The FDs were small for those compounds exhibiting a large roughness number and those in a large order.

Subsequently, the performance of the proposed REFD FW algorithm was evaluated. A classical comparison analysis based on emulated noisy image was conducted by using a high quality image as the original, adding Gaussian white noise of a given variance σ to the original image, and then approximating the original image from the noisy one by using the denoising method. This study involved using three side-scan sonar images of a pipeline that were captured using the Polaris camera(Taiwan),as shown in Fig.8, as the experimental objects. The images were enlarged to 2048×2048 pixels and transformed to 8-bit gray images, and then Gaussian white noise (at zero mean and variance σ = 0.01) was added to the original sonar image to be the noisy image. The REFD FW algorithm and a slightly modified generic FW scheme were then employed to reduce noises in the noisy sonar images.

In addition, the proposed method was compared with a generic FW compression algorithm introduced by Avanakiet al. [23]. Table 3 shows that the results obtained from applying the derived FD values of the REFD were superior to those obtained from the generic FW algorithm.

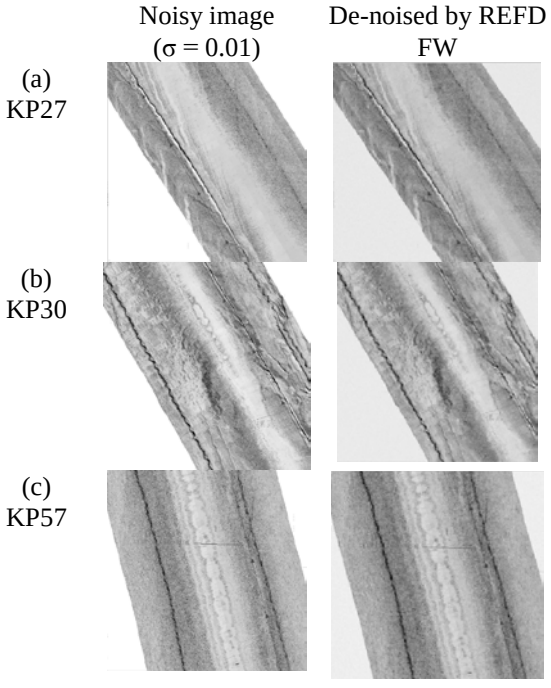


Fig. 8. De-noising effects for sonar image of the pipeline exposure and free span taken by the Polaris.

Table 3.

The MSE and PSNR values for the noisy sonar image after de-noising

| | | σ = 0.01 | | | σ = 0.05 | | | σ = 0.1 | | |
|---|---|---|---|---|---|---|---|---|---|---|
| | | (a) KP27 | (b) KP30 | (c) KP57 | (a) KP27 | (b) KP30 | (c) KP57 | (a) KP27 | (b) KP30 | (c) KP57 |
| Noisy image (before de-noising) | MSE | 40693 | 38852 | 34150 | 40712 | 38871 | 34168 | 40727 | 38886 | 34181 |
| | PSNR (dB) | 2.070 | 2.271 | 2.831 | 2.068 | 2.269 | 2.829 | 2.07 | 2.267 | 2.827 |
| The REFD FW algorithm | MSE | 151 | 229 | 187 | 297 | 358 | 270 | 503 | 553 | 396 |
| | PSNR (dB) | 26.37 | 24.57 | 25.45 | 23.43 | 22.63 | 23.86 | 21.15 | 20.74 | 22.18 |
| FW coding [25] | MSE | 40682 | 38851 | 34147 | 40683 | 38852 | 34148 | 40684 | 38853 | 34150 |
| | PSNR (dB) | 2.071 | 2.271 | 2.831 | 2.070 | 2.270 | 2.831 | 2.066 | 2.271 | 2.831 |

# 4 Conclusion

This study proposed a FWdenoising alternative based on applying a texture analysis technique to the fractal matching process. The performance of the REFD FW algorithm was determinedby applying it on a sonar image. Ananalysis of theproposed algorithm based on texture similarityrevealedthe adaptability of the algorithm in denoisingside-scan sonarimages.

## Acknowledgment

This study was supported by the National Science Council of Taiwan, R.O.C. under contracts NSC 102-2221-E-146-004. The authors gratefully acknowledge M.R.N. Avanaki, Hamid Ahmadinejad, and Reza Ebrahimpour for providing us with the MATLAB program Wavelet Fractal Compression that was used for the experiments.

*References:*

[1] D. Krotser, and M. Klein, “Side-Scan Sonar: Selective Textural Enhancement,” IEEE Conference on OCEANS '76 ,pp.445-450 ,1976.

[2] K. Enomoto, M. Toda, and Y. Kuwahara “Extraction Method of Scallop Area in Gravel Seabed Images for Fishery Investigation” IEICE TRANSACTIONS on Information and Systems, vol. E93-D no.7pp.1754-1760, 2010

[3] H.-W. Tin, S.-W.Leu, F.-T. Wang, C.-C. Wen, and S.-H. Chang, "Denoising Algorithm Based on Fractal-Wavelet coding and its Application to Side-scan Sonar Image," 2013 International Symposium on Physics and Mechanics of New Materials and Underwater Applications (PHENMA 2013), pp.30, June, 2013.

[4] G. J. Orris, B. E. McDonald, and W. A. Kuperman, "Matched-phase noise reduction," J. Acoust. Soc. Amer., vol. 96, no. 6, pp. 3499-3503, Dec. 1994.

[5] A. Jarrot, C. Ioana, and A. Quinquis, "Denoising underwater signals propagating through multi-path channels," in Proc. Oceans 05 Europe, Brest, France, pp. 501-506, Jun. 2005.

[6] M. Jansen, Noise Reduction by Wavelet Thresholding. NewYork: Springer Verlag, 2000, vol. 161.

[7] D. L. Donoho, "De-noising by soft-thresholding," IEEE Trans. Inf. Theory, vol. 41, no. 3, pp. 613-627, 1995.

[8] A. Malviya, "Fractal based spatial domain techniques for image de-noising," International Conference on Digital Object Identifier, pp.1511 – 1516, 2008.

[9] M. Ghazel, G. Freeman, and E. R. Vrscay, "Fractal-wavelet Image Denoising Revisited, " IEEE Transactions on Image Processing, vol.15, pp. 2669-2675 ,2006.

[10] J. Lu, Y. Zou, and Z. Ye , "Enhanced Fractal-Wavelet Image Denoising," ISECS International Colloquium on Computing, Communication, Control, and Management (CCCM '08), pp. 115 – 119,2008.

[11] H.-W. Tin , S.-W.Leu , C.-C. Wen, and S.-H. Chang, "An Efficient Sidescan Sonar Image Denoising Method Based on a New Roughness Entropy Fractal Dimension,"International Symposium on Underwater Technology 2013, March, 2013.

[12] B. B. Chaudhuri and N. Sarkar, "Texture segmentation using fractal dimension," IEEE Trans. Pattern Anal. Mach. Intell., vol. 17, no. 1, pp.72-77, 1995.

[13] L.M. Linnett, D.R. Carmichael, S.J. Clarke, A.D. Tress, "Texture analysis of sidescan sonar data," IEE Seminar on Texture analysis in radar and sonar, pp.2/1-2/6, 1993.

[14] B.B. Mandelbrot, Fractal Geometry of Nature, San Francisco, CA: Freeman ,1982.

[15] A.E. Jacquin, "Image Coding Based on a Fractal Theory of Iterated Contractive Image Transformations," IEEE Trans. Image Processing, pp.18-30 ,1992.

[16] M.F. Barnsley, S. Demko, "Iterated function systems and global construction of fractals," Proceedings of the Royal Society of London, pp.243-275 ,1985.

[17] H.-W. Tin, S.-W. Leu, and S.-H. Chang, "An PSO-based Approach to Speed up the Fractal Encoding", International Journal of Mathematical Models and Methods in Applied Sciences,Vol.6, pp. 499-506, 2012.

[18] H.-W. Tin, S.-W. Leu, H. Sasaki, and S.-H. Chang, "A Novel Fractal Block Coding Method by Using New Shape-Based Descriptor", Applied Mathematics & Information Sciences, (Accepted), 2013 .

[19] A. Pentland and B. Horowitz, "A practical approach to fractal-based image compression, " in Proc. Data Compression Conf., Snowbird, UT, pp. 176-185 ,1991.

[20] G.M. Davis, "A Wavelet-Based Analysis of Fractal Image Compression," IEEE Trans. Image Processing, vol. 7, pp.141-154 ,1998.

[21] Y. Fisher, Fractal Image Compression-Theory and Application, NewYork: Springer Verlag, 1995.

[22] Strahler, A. N., Quantitative analysis of watershed geomorphology, Am. Geophys. Union Trans., pp.913-920, 1957.

[23] R. E. Horton, "Erosional development of streams and their drainage basins: hydrophysical approach to quantitative morphology," Bull.Geol. Soc. Am., pp.275-370, 1945.

[24] S. Frontier, "Applications of Fractal theory to Ecology, " Legendre, P., Legendre, L. (Eds.), Developments in Numerical Ecology, pp.335-378, 1987.

[25] M.R.N. Avanaki, H. Ahmadinejad, R. Ebrahimpour, "Evaluation of Pure-Fractal and Wavelet-Fractal Compression Techniques, " International Journal on Graphics, Vision and Image Processing, vol. 9, issue IV, pp. 41-47, 2009.